HHS Public Access

Author manuscript

Neuron. Author manuscript; available in PMC 2017 April 06.

Published in final edited form as:

Neuron. 2016 April 6; 90(1): 43–55. doi:10.1016/j.neuron.2016.02.021.

Psychiatric Risk Gene Transcription Factor 4 Regulates Intrinsic Excitability of Prefrontal Neurons via Repression of SCN10a and KCNQ1

Matthew D. Rannals[1], **Gregory R. Hamersky**[1], **Stephanie Cerceo Page**[1], **Morganne N. Campbell**[1], **Aaron Briley**[1], **Ryan A. Gallo**[1], **BaDoi N. Phan**[1], **Thomas M. Hyde**[1,2,5,6], **Joel E. Kleinman**[5], **Joo Heon Shin**[1], **Andrew E. Jaffe**[1,4,5], **Daniel R. Weinberger**[1,2,3,6], and **Brady J. Maher**[1,2,3,*]

[1]Lieber Institute for Brain Development, Johns Hopkins Medical Campus, Baltimore, MD, 21205, USA

[2]Department of Psychiatry and Behavioral Sciences, Johns Hopkins School of Medicine, Baltimore, MD, 21287, USA

[3]Department of Neuroscience, Johns Hopkins School of Medicine, Baltimore, MD, 21205, USA

[4]Department of Biostatistics, Johns Hopkins Bloomberg School of Health, Baltimore, MD, 21205, USA

[5]Department of Mental Health, Johns Hopkins Bloomberg School of Public Health, Baltimore, MD, 21205, USA

[6]Department of Neurology and the McKusick Nathans Institute of Genetic Medicine, Johns Hopkins School of Medicine, Baltimore, MD, 21205, USA

Summary

Transcription Factor 4 (TCF4) is a clinically pleiotropic gene associated with schizophrenia and Pitt-Hopkins syndrome (PTHS). To gain insight about the neurobiology of TCF4, we created an *in vivo* model of PTHS by suppressing *Tcf4* expression in rat prefrontal neurons immediately prior to neurogenesis. This cell-autonomous genetic insult attenuated neuronal spiking by increasing the afterhyperpolarization. At the molecular level, using a novel technique called iTRAP that combined *in utero* electroporation and translating ribosome affinity purification, we identified increased translation of two ion channel genes, *Kcnq1* and *Scn10a*. These ion channel candidates

*Correspondence: brady.maher@libd.org.

AUTHOR CONTRIBUTIONS

M.D.R. contributed to all aspects of experiments, electrophysiology and data analysis; S.C.P. performed confocal imaging; M.N.C. performed *in vitro* validation of shRNA and CRISPR-Cas9 constructs and qRT-PCR; G.R.H. performed electrophysiology experiments; A.B. cloned and validated shRNA constructs; R.A.G. cloned and validated CRISPR-Cas9 constructs; A.E.J. performed statistical analysis and RNAseq; A.E.J and B.N.P. performed ChIPseq analysis; T.M.H. and J.E.K. contributed RNAseq data; J.H.S performed RNAseq; D.R.W. contributed to writing and supervised RNAseq; B.J.M contributed to all aspects of experiments, electrophysiology, experimental design, writing and data analysis.

were validated by pharmacological rescue and molecular phenocopy. Remarkably, similar excitability deficits were observed in prefrontal neurons from a *Tcf4*$^{+/tr}$ mouse model of PTHS. Thus, we identify TCF4 as a regulator of neuronal intrinsic excitability in part by repression of *Kcnq1* and *Scn10a*, and suggest this molecular function may underlie pathophysiology associated with neuropsychiatric disorders.

INTRODUCTION

Pitt-Hopkins syndrome (PTHS) and 18q syndrome are rare neurodevelopmental disorders characterized by intellectual disability, failure to acquire language, deficits in motor learning, hyperventilation, epilepsy, autistic behavior, and gastrointestinal abnormalities (Whalen *et al.* 2012; Forrest *et al.* 2012; Sweatt 2013; Soileau *et al.* 2014). PTHS is caused by a variety of mutations of *TCF4* (*ITF2*, *SEF2*, *E2-2*), each of which results in TCF4 protein deficiency (Brockschmidt *et al.* 2011; Zweier *et al.* 2008; Amiel *et al.* 2007; Sepp *et al.* 2012). In addition, single nucleotide polymorphisms (SNPs) in a genomic locus containing *TCF4* were among the first to reach genome-wide significance in clinical genome-wide association studies (GWAS) for schizophrenia (Schizophrenia Psychiatric Genome-Wide Association Study (GWAS) Consortium 2011), and are strongly significant in the most recent GWAS ($p=9.09\times10^{-13}$; (Schizophrenia Working Group of the Psychiatric Genomics Consortium 2014). These neuropsychiatric disorders are each characterized by prominent cognitive deficits, which suggest not only genetic overlap between these disorders but a potentially overlapping pathophysiology.

TCF4 is a basic helix-loop-helix (bHLH) transcription factor (TF) that forms homo- or heterodimers with itself or other bHLH TFs (Henthorn *et al.* 1990; Corneliussen *et al.* 1991). Dimerization allows for recognition of E-box binding sites (motif: CANNTG), and direct DNA binding can result in either repression or activation of transcription depending on the protein complex bound to TCF4 (Massari and Murre 2000). *TCF4* is highly expressed throughout the CNS during human development (de Pontual *et al.* 2009), but regulation of expression and splicing is complex, as multiple alternative transcripts containing different 5′ exons and internal splicing have been identified (Sepp *et al.* 2011). Limited understanding also exists for the genes regulated downstream of TCF4 and this is complicated by the limited specificity of the E-box sequence as well as context-dependent regulation due to heterodimerization, developmental expression and cell-type specificity (Guillemot 2007; Powell and Jarman 2008).

To unravel the biology of TCF4 and to gain insight into the pathophysiology resulting from *TCF4* haploinsufficiency, we developed an *in vivo* cell-autonomous model of PTHS, using *in utero* electroporation (IUE) to knockdown the expression of *Tcf4* beginning just prior to neurogenesis in the developing rat prefrontal neocortex. We report here that this genetic manipulation produces intrinsic excitability defects that result from de-repression of the expression of specific ion channel genes that are known to regulate the frequency of action potential (AP) spiking. In addition, these excitability phenotypes were replicated in a mouse model of PTHS. We propose that these intrinsic excitability phenotypes may underlie some

aspects of pathophysiology observed in PTHS and schizophrenia and identify potential ion channel therapeutic targets.

RESULTS

The developmental expression pattern of *TCF4* across the lifespan is similar between humans and rodents

We sought to more precisely characterize the developmental expression patterns of *TCF4* in both rat and human to determine critical periods of expression. We observed analogous expression trajectories in both human and rat suggesting developmental regulation of TCF4 may be similar between species. *TCF4* mRNA expression peaks in late prenatal life, corresponding to the third trimester of fetal life in humans and postnatal day 1 (P1) in rat, and declines during early childhood before leveling off into adulthood (Figure 1A). The rapid rise in *TCF4* transcripts during corticogenesis likely implicates a critical time period for TCF4 biology.

Validation of shRNA constructs to create a cell-autonomous model of TCF4 haploinsufficiency

To gain insight into the function of TCF4 during this prenatal peak in expression and to create a cellular model of PTHS, we designed and validated two shRNA constructs to specifically knockdown *Tcf4 in utero* at embryonic day 16 (E16) just prior to its rise in late prenatal life. Each shRNA construct targets a unique region of the rat *Tcf4* transcript, shTCF4 targets a common 3′ exon found in all known *Tcf4* isoforms and shTCF4_2 targets a common 3′UTR. Both shRNA constructs were validated *in vitro* and showed consistent knockdown of endogenous *Tcf4* mRNA ($p<0.002$) and TCF4 protein ($p<0.0001$) in transfected rat neuroblastoma cells compared to a control shRNA (shCon) that does not target any known rat sequence but is processed by the cell into an interfering RNA (Figure 1B–E).

Our electroporation targeted the medial prefrontal cortex (mPFC), which is the generally accepted rodent homologue of human prefrontal association cortex, an important brain region associated with cognitive deficits in psychiatric disorders (Goldberg and Weinberger 1988; Goldman-Rakic 1994; Goldman-Rakic 1995). An example image of our mPFC electroporation is shown in Figure S1. TCF4 knockdown by shTCF4 did not produce any gross morphological defects in neuronal migration or morphology (Figure S1).

TCF4 regulates the intrinsic excitability of prefrontal cortical neurons

To determine if *in utero* suppression of TCF4 negatively impacts the physiology of cortical neurons, we assayed intrinsic excitability by performing whole-cell recordings from IUE transfected neurons and measured the frequency of AP spiking elicited by a series of depolarizing current pulses. TCF4 knockdown produced a severe and consistent reduction of AP output frequency compared to shCon cells (Figure 2A,B; $p<0.0001$). The maximum frequency of spikes elicited by any size current pulse for each cell was also significantly reduced by both TCF4 shRNA constructs (Figure 2C; $p<0.0001$). We obtained several other intrinsic excitability measurements from these recordings (Figure S2, Table S1) and the only

consistent effect observed between both shTCF4 and shTCF4_2 was an increase in the resting membrane potential (RMP, Figure S2A; $p<0.0001$) and the peak amplitude of the AP (Figure S2G,H; $p<0.0003$). Consistent with these and other intrinsic excitability deficits, we also observed an increased variance of AP amplitudes in response to simulated trains of synaptic inputs (Figure S2).

Targeted knockdown of gene expression by RNA interference is potentially complicated by off-target knockdown due to sequence-dependent and sequence-independent effects (Alvarez *et al.* 2006; Baek *et al.* 2014). In addition to showing phenotypic overlap using two independent TCF4 shRNA constructs, we controlled for sequence-dependent effects by performing rescue experiments. Co-expression of human TCF4B + shTCF4 resulted in a complete rescue of AP output (Figure 2B,C). To control for sequence-independent off-targets effects we designed a CRISPR-Cas9 construct to mutate/knockout *Tcf4* (crTCF4). *In vitro* validation of crTCF4 in transfected rat neuroblastoma cells showed it was effective at making targeted mutations in the *Tcf4* locus as measured by the SURVEYOR nuclease assay (Figure S3A) and was effective at knockdown of endogenous TCF4 (Figure S3C). crTCF4 was delivered via IUE and produced a significant reduction in the frequency neuronal spiking compared to crEmpty cells (Figure 2D,E; $p<0.0001$). Maximum spiking frequency analysis showed that crTCF4 cells had significantly reduced AP output compared to crEmpty cells ($p=0.0016$). Phenocopy by crTCF4 indicates that the altered intrinsic excitability associated with shRNA suppression of TCF4 is primarily due to disruption of TCF4 signaling and not the result of off-target effects.

TCF4 regulates the afterhyperpolarization in mPFC neurons

To more fully characterize the molecular mechanism responsible for the reduction of AP output in shTCF4 neurons, we measured the afterhyperpolarization current (AHP) that regulates neuronal spike frequency. Ca^{2+}-activated potassium channels hyperpolarize the membrane, making it less likely that neurons will reach threshold and fire subsequent APs (Hille 2001; Sah and Louise Faber 2002; Vogalis *et al.* 2003; Bean 2007). Several K^+ channel conductances are responsible for producing the AHP and they are characterized by their kinetics such that the AHP consists of a fast (fAHP), medium (mAHP) and slow component (sAHP) (Sah and Louise Faber 2002). Because the mAHP and sAHP are inversely correlated with average firing rate and the amplitude of the sAHP depends on the number of spikes (Lorenzon and Foehring 1995; Abel 2003), we measured the mAHP and sAHP from traces showing spiking frequencies of 12±1.0Hz (Figure 2C), which corresponds to the median of the maximum spiking for shTCF4 cells. Both the mAHP ($p<0.0001$) and sAHP ($p=0.0003$) were significantly larger in shTCF4 cells compared to shCon cells (Figure 3B,C). We did not find a significant difference in the fAHP between shTCF4 and shCon cells ($p=0.33$). In addition, we observed the mAHP ($p=0.029$), but not the sAHP ($p=0.28$) was larger in crTCF4 cells compared to crEmpty cells (Figure S3). These results indicate that TCF4 regulates neuronal output spiking through its control of the AHP.

To further validate the role of TCF4 in regulating the AHP and to more precisely pinpoint the underlying conductances responsible for the increase in the AHP, we conducted voltage-clamp experiments to isolate specific Ca^{2+}-activated K^+ channel currents. We observed that

shTCF4 neurons displayed significantly larger capacitance normalized charge transfer compared to shCon neurons (p=0.008). Progressive pharmacological blockade was then used to isolate specific components of the AHP. The fAHP is primarily produced by the large conductance calcium-activated big potassium channels (BK) and is blocked by the nonselective antagonist TEA (1mM). We observed the AHP current from TCF4 knockdown neurons remained significantly increased in the presence of TEA (Figure 3E,G; p=0.0096). The mAHP is produced by the small conductance Ca^{2+}-activated potassium channels (SK) and is selectively sensitive to apamin (Sah and Louise Faber 2002). Application of apamin (100nM) blocked the mAHP in both conditions, and the remaining sAHP current was still significantly increased in shTCF4 cells compared to shCon cells (Figure 3F,G; p=0.013). Because apamin is highly selective for SK channels, we subtracted the AHP current traces generated before and after its application to isolate the apamin-sensitive component (Figure 3H). This subtraction did not reveal a significant difference (p=0.53) in the apamin-sensitive current between our conditions (Figure 3I), suggesting that SK channel expression does not appear to be altered by TCF4 knockdown. From these results the exact identity of the responsible conductance could not be determined, however these data replicate our current-clamp results (Fig. 3A–C) and strengthen the conclusion that TCF4 is regulating neuronal spiking via the AHP.

TCF4 regulates the expression of KCNQ1 and SCN10a

While we identified that TCF4 significantly associates with the AHP (Figure 3), our voltage-clamp experiments did not identify the exact conductance(s) regulated by TCF4. We therefore used molecular profiling to identify the particular genes responsible for the intrinsic excitability phenotype by adapting translating ribosome affinity purification (TRAP) (Heiman *et al.* 2008; Heiman *et al.* 2014) for use with IUE, in a novel approach we term “iTRAP”. We co-expressed the EGFP-fused ribosomal protein L10a-EGFP with either shTCF4 or shCon and performed affinity purification from IUE transfected mPFC brains on P21. A major advantage of this technique is that IUE specifically transfects a homogenous population of layer specific excitatory neurons (Langevin *et al.* 2007), and we validated that iTRAP enriches for excitatory neurons by comparing the expression of cell-type specific markers between our EGFP affinity-bound RNA fraction and unbound RNA fraction. Consistent with excitatory neuronal enrichment, we observed an approximate 2-fold decrease in the expression of *GAD1* (p=0.007), *GFAP* (p=0.01), and *OLIG1* (p=0.0003) in our EGFP-bound fraction compared to unbound fraction (Figure 4B). In addition, we observed a greater than 400-fold increase in the expression of EGFP (p=0.0006). We next compared the ion channel translatome of TCF4 knockdown neurons to shCon neurons using prefabricated 384-well qPCR plates containing the majority of known ion channel genes in the rat genome. This analysis revealed only two ion channel genes, *Kcnq1* (Kv7.1; p<0.005) and *Scn10a* (Nav1.8; p<0.01) that were significantly upregulated in shTCF4 neurons compared to shCon neurons. We demonstrated that enrichment via the iTRAP protocol was required because *Kcnq1* and *Scn10a* expression was not significantly different when measured from total RNA from whole frontal cortex homogenates (Figure S4). Remarkably, both of these genes have previously been implicated in regulating spike frequency adaptation (Delmas and Brown 2005; Blair and Bean 2003) and thus are strong candidate genes underlying our excitability phenotype.

To determine if TCF4 directly binds to *KCNQ1* and *SCN10a* we first analyzed the publicly available ENCODE datasets of TCF4 ChIP-seq performed in human K562 cell line (Consortium 2012). After aligning the raw reads to the genome and calling peaks (Ji *et al.* 2008), we identified two genome-wide significant (at FDR < 5%) peaks in both of these genes. In *KCNQ1*, both peaks (chr11:2799700-2800099, FDR = 0.005 and chr11:2760400-2760749, FDR = 0.013) were located in intronic sequence, and both contained multiple canonical E-box binding motifs (CANNTG, first peak: 2, second peak: 9). Similarly, in *SCN10a*, both peaks (chr3:38765550-38766049, FDR < 1×10^{-4} and chr3:38767100-38767499, FDR < 1×10^{-4}) were located in intronic sequence and both contained multiple canonical E-box binding motifs (CANNTG, first peak: 2, second peak: 6).

We then performed ChIP-seq of endogenous TCF4 in rat neuroprogenitor cell cultures to confirm these results in our rodent system. We again found multiple significant peaks in both genes (compared to an untreated input sample, see Methods), including 12 genome-wide significant peaks in and around (within 20kb) *Kcnq1* and 4 genome-wide significant peaks in and around *Scn10a* (Table S2). These results in both human and rat indicate TCF4 directly binds to genomic regions within *KCNQ1* and *SCN10a* and suggests TCF4 could directly regulate the expression of these genes.

Molecular and pharmacological validation of SCN10a and KCNQ1 as candidate genes associated with TCF4-dependent regulation of intrinsic excitability

To validate our iTRAP experiment and to further understand the underlying molecular mechanism responsible for the TCF4-dependent effects on intrinsic excitability, we utilized pharmacological and molecular methods to both rescue and phenocopy our shTCF4 phenotypes. UCL2077 and JNJ303 are two competitive antagonists with selectivity for KCNQ potassium channels (Towart *et al.* 2009; Soh and Tzingounis 2010). UCL2077 is a KCNQ subtype-selective blocker that strongly inhibits KCNQ1 and KCNQ2 (Soh and Tzingounis 2010), whereas JNJ303 is a potent KCNQ1 antagonist (IC_{50}=64nM) with unknown subtype selectivity (Towart *et al.* 2009). We tested these antagonists using a within neuron design and observed that both UCL2077 (p=0.0002; CrTCF4 p=0.045, Figure S5) and JNJ303 (p=0.0084) were effective at increasing the spiking frequency in shTCF4 neurons (Figure 5). Importantly, neither UCL2077 (p=0.35) nor JNJ303 (p=0.11) had an effect on spiking in shCon cells (Figure 5C,F; UCL2077 on crEmpty cells p=0.99, Figure S5C). In addition, we measured the amplitudes of the mAHP and sAHP before and after application of UCL2077 or JNJ303. Consistent with increased *Kcnq1* expression contributing to the AHP amplitude, UCL2077 and JNJ303 were both effective at reducing both the mAHP (UCL2077 p=0.003; JNJ303 p=0.044) and sAHP (UCL2077 p=0.039, JNJ303 p=0.041) amplitudes in shTCF4 neurons. Notably and coherent with spike frequency data, neither UCL2077 nor JNJ303 had any consistent effect on the amplitudes of the mAHP (UCL2077 p=0.89; JNJ303 p=0.40) or sAHP (UCL2077 p=0.91, JNJ303 p=0.20) in shCon cells. These pharmacological results suggest reduced firing frequencies observed in shTCF4 neurons are associated with enhanced KCNQ1 expression that result in a subsequent increase in the amplitude of the AHP.

To validate SCN10a, we first overexpressed a recombinant *Scn10a* construct to phenocopy TCF4 knockdown. We used IUE to co-transfect *Scn10a* + shCon and remarkably, this manipulation resulted in a consistent phenocopy of the intrinsic excitability deficits observed with TCF4 suppression. *Scn10a* + shCon expression produced a significant decrease in spiking frequency compared to shCon cells (Figure 6B; $p<0.0001$), and also depolarized the RMP ($p<0.0001$) to a similar magnitude observed in TCF4 knockdown cells (Figure 6C and Figure S2). Bath application of a selective SCN10a antagonist (A-803467; 200nM) was effective at increasing firing frequency in shTCF4 cells (Figure 6D, $p<0.05$) and crTCF4 cells (Figure S5, $p=0.039$). Importantly, A-803467 had no effect on firing frequency in shCon cells ($p=0.14$) or crEmpty cells ($p=0.15$, Figure S5D). The selective effect of A-803467 only on shTCF4 and crTCF4 cells suggests SCN10a is overexpressed in these neurons.

To further rule out the potential of nonspecific pharmacology of antagonists to both KCNQ1 and SCN10a, we designed and validated CRISPR-Cas9 constructs that target both *Kcnq1* and *Scn10a* (Figure 6F). Co-expression of crKCNQ1, crSCN10a and shTCF4 resulted in complete rescue of AP spike output (Figure 6G; $p<0.0001$). Together these results robustly validate our iTRAP method and suggest that under normal conditions, TCF4 represses the expression of KCNQ1 and SCN10a in layer 2/3 neurons of the rat prefrontal cortex.

Phenocopy in a mouse model of PTHS

We next sought to validate the intrinsic excitability phenotypes we have observed in our cell-autonomous model of PTHS in a mouse model in which we measured input-output curves from mPFC neurons (Sweatt 2013; Grubišić *et al.* 2015). This mouse model was created by insertion of a neo cassette into EcoRV sites within the bHLH domain of *Tcf4* (Figure S7), and was originally believed to result in a constitutive deletion of one allele of the *Tcf4* gene, thus modeling germline *TCF4* haploinsufficiency (Zhuang *et al.* 1996). To validate this model at the protein level we performed Western blots from embryonic day 18 (E18) embryos and observed a truncated protein band that was dependent on genotype (Figure 7A), suggesting the presence of a potentially dominant-negative protein (Sepp *et al.* 2012). Remarkably, whole-cell recordings in layer 2/3 neurons from $Tcf4^{+/tr}$ brain slices produced a severe and consistent reduction of spike output (Figure 7B,C; $p<0.0001$) and the maximum number of spikes elicited by any size current pulse for each cell was also significantly reduced compared to recordings from $Tcf4^{+/+}$ littermates (Figure S6; $Tcf4^{+/tr}$ 24.4±1.1Hz, N=27 vs. $Tcf4^{+/+}$ 29.9±1.1 Hz, N=24, $p<0.007$). $Tcf4^{+/tr}$ cells also displayed a significantly depolarized RMP compared to $Tcf4^{+/+}$ littermates (Figure 7D; $p=0.0037$). In contrast to our cell-autonomous model, both the mAHP ($Tcf4^{+/tr}$ −4.9±0.5mV, N=46 vs. $Tcf4^{+/+}$ −5.6±0.5mV, N=35, $p<0.31$) and sAHP ($Tcf4^{+/tr}$ −3.4±0.4mV, N=46 vs. $Tcf4^{+/+}$ −4.4±0.4mV, N=35, $p<0.15$) amplitudes were slightly decreased, but not significantly different, between $Tcf4^{+/tr}$ and $Tcf4^{+/+}$ recordings. The remarkable phenotypic overlap between our two model systems suggests deficits in AP output may represent a true pathophysiological state in PTHS, however the subtle differences between our model systems may indicate different underlying mechanisms may exist.

If the truncated TCF4 protein that is expressed in this mouse model is capable of binding to wild-type TCF4 protein in a dominant-negative fashion, this could likely lead to different cellular and molecular mechanisms being responsible for the excitability phenotypes observed in our two PTHS models. Therefore, we measured total RNA from frontal cortex homogenates from *Tcf4*$^{+/tr}$ and *Tcf4*$^{+/+}$ littermates and consistent with our electrophysiological results, we observed a significant 246±0.5% increase in *Scn10a* (p=0.027) expression but only a 32±0.2% decrease in *Kcnq1* (p=0.015) expression (Figure 7G). To determine if these expression differences translate to physiological differences, we tested the effects of SCN10a and KCNQ1 antagonists on AP output. The SCN10a antagonist A-803467 was effective at rescuing AP output in TCF4$^{+/tr}$ cells but the KCNQ1 antagonist UCL2077 had no effect (Figure 7I). These results confirm a role of SCN10a in the intrinsic excitability phenotype in this PTHS mouse model.

Discussion

We have performed a series of experiments to illuminate the role of TCF4 as a susceptibility factor in neurodevelopmental psychiatric disorders, specifically describing the biological function and the pathophysiological consequence of TCF4 haploinsufficiency and dominant-negative isoforms associated with PTHS. We developed a novel *in vivo* cellular model that mimics aspects of *TCF4* expression observed in PTHS. We show isomorphic expression trajectories in the human DLPFC and rat cortex across the lifespan, identifying a peak of *TCF4* expression during cortical development that subsides during the postnatal period. Based on this early expression pattern, we established a developmental cellular assay by using IUE to knockdown of *Tcf4* expression just prior to the peak of *Tcf4* expression in the rat. We propose that this creates a cell-autonomous model of PTHS.

Using this approach, we have identified a novel and robust function of TCF4 in the regulation of intrinsic excitability of prefrontal neurons. We show that *in utero* suppression of TCF4 significantly affects excitability by increasing the magnitude of the AHP and reducing AP output. To identify the molecular mechanisms for these phenotypes we developed iTRAP, a new molecular profiling technique that provides access to the translatome of IUE transfected cortical neurons. In the past, experiments using IUE have been hampered by the mosaic expression pattern produced by electroporation and the inability to selectively isolate transfected cells for molecular or biochemical profiling. iTRAP overcomes this technical issue and opens the door for future mechanistic studies on the function of genes associated with neuropsychiatric disorders. By comparing the translatome between shTCF4 and shCon neurons with iTRAP, we identified significant upregulation of *Kcnq1* and *Scn10a* translation. Analysis of two independent TCF4 ChIP-seq data (Consortium 2012) showed direct binding of TCF4 to genomic regions within *KCNQ1* and *SCN10a*, indicating direct regulation of these genes by TCF4.

KCNQ1 is a member of the KCNQ gene family, which encodes five voltage-gated, delayed rectifier K^+ channels (KCNQ1 to KCNQ5; Kv7.1 to Kv7.5) known to be the molecular components of the M-current (Delmas and Brown 2005). Consistent with our results, the KCNQ family appears to contribute to the sAHP (Tzingounis *et al.* 2007; Tzingounis and Nicoll 2008; Soh and Tzingounis 2010). We show that the KCNQ1 antagonists UCL-2077

and JNJ-303 were effective at blocking the mAHP and sAHP, and this resulted in rescue of spike frequency in shTCF4 cells. Importantly, this effect was selective to shTCF4 cells and not shCon cells. While KCNQ1 selectivity of UCL2077 is known, the selectivity for KCNQ1 of JNJ-303 over other KCNQ subunits is not reported, but our results would indicate it is similarly selective. It is known that KCNQ channels activate slowly upon depolarization (Jentsch 2000), and neuron modeling indicates the AHP amplitude is increased at depolarized RMPs (Gu *et al.* 2005). We observed in the majority of our genetic manipulations that the RMP is depolarized when TCF4 is suppressed (Table S1) and this effect may be favorable to enhancing KCNQ1 currents, however holding shTCF4 cells at more hyperpolarized RMPs had no effect on AP output ($ANOVA_{RMP}$ p=0.48) or the AHP amplitude (mAHP p=0.73; sAHP p=0.87). Together, these results confirm our iTRAP molecular profiling experiments and suggest TCF4 is regulating the expression of KCNQ1 in L2/3 pyramidal cells.

SCN10a (NaV1.8) is a peripherally expressed, TTX-resistant, voltage-gated Na^+ channel that shows prominent slow inactivation (Vijayaragavan *et al.* 2001) shown to be responsible for spike-frequency adaptation in dorsal root ganglion neurons (Blair and Bean 2003). We validated TCF4 regulation of SCN10a by showing *Scn10a* overexpression resulted in phenocopy of RMP and action potential output. In addition, a specific NaV1.8 antagonist (A-803467) showed selective rescue only in shTCF4 cells. The exact biophysical mechanism responsible for this phenocopy is not known. To our knowledge wild-type SCN10a is not known to regulate the RMP, however a *SCN10a* point-mutant (I1706V) found in a patient with idiopathic small-fiber neuropathy lead to a depolarized RMP in dorsal root ganglion cells (Huang *et al.* 2013). It is reasonable to infer that increasing the expression of a sodium channel would favor a more depolarized RMP. The effect of SCN10a on AP output likely involves slow inactivation of the channel during a train of APs (Blair and Bean 2003). It is important to note that TTX resistant Na^+ currents are thought to be only expressed in the peripheral nervous system (Baker and Wood 2001; McCleskey and Gold 2003), and to our knowledge this is the first report of a role of expression of S*cn10a* in the central nervous system despite suggestions that *SCN10a* mRNA is present at low levels in the mouse and human neocortex (Lein *et al.* 2007; Hawrylycz *et al.* 2012).

As further validations of the intrinsic excitability phenotypes we found in our cell-autonomous model of PTHS, we observed similar deficits in AP output in a mouse model of PTHS in which one allele of *Tcf4* produces a truncated TCF4 protein. This mouse model, more closely matches the molecular biology of PTHS (Sweatt 2013) and therefore may provide more meaningful representation of pathophysiology in PTHS. Homozygous deletion of TCF4 is lethal at birth and defects in progenitor cell migration in the pontine nucleus are reported (Flora *et al.* 2007). Heterozygous mice, which model the genetic abnormality of PTHS in humans, exhibit abnormal gut function, the most common non-neurological symptom in PTHS patients (Grubišić *et al.* 2015), and thus substantiates this mouse as a model of at least some fundamental aspects of PTHS.

Although deficits in AP output was a consistent phenotype observed in every experimental approach and between two model systems, we did observe some variability in the data (Table S1). This variability is not unexpected and is likely due to differences in the specific

mechanism of action that each molecular approach targets (i.e. at the level of DNA, RNA, or protein), their varying magnitude of effect on TCF4 expression, and the known heterogeneity within pyramidal cells of layer 2/3 (Tyler *et al.* 2015). Therefore, we believe this variability is peripheral to the consistently observed result that TCF4 regulates spike frequency through regulation of SCN10a as demonstrated using pharmacological and molecular rescue and phenocopy.

It is also noteworthy that the underlying mechanism was only partially consistent between our rat and mouse models. This mechanistic difference is likely attributable to model construction, as shTCF4 and crTCF4 produce haploinsufficiency while expression of a truncated TCF4 protein is likely a dominant-negative. The divergent expression of *Kcnq1*, yet similar expression of *Scn10a*, between these two models indicates transcriptional control by TCF4 is different depending on the gene being regulated and is consistent with context-dependence of bHLH proteins (Powell and Jarman 2008). From our data, we would predict *Scn10a* and Kcnq1 are differentially regulated by TCF4 through its ability to form homo- or heterodimers and this may explain the varied symptomology observed in the PTHS patient population. The physiological abnormalities we observe in the cortex of these mice implicate an abnormality of neuronal excitability as a possible mechanism of the cognitive disability also observed in this condition. Moreover, the consistency of the excitability phenotypes between the mouse model and the cell-autonomous model support the conclusion that TCF4 is a regulator of intrinsic neuronal excitability and that *Scn10a* is at least in part a factor in mediating this effect.

TCF4 is linked to several neuropsychiatric disorders including schizophrenia, PTHS, and 18q deletion syndrome. For schizophrenia, common variants, some within introns of *TCF4*, have reached genome-wide significance for association with diagnosis (Schizophrenia Psychiatric Genome-Wide Association Study (GWAS) Consortium 2011). In addition, several *TCF4* SNPs including some risk SNPs, are associated with SZ endophenotypes including cognition and sensorimotor gating (Zhu *et al.* 2012; Quednow *et al.* 2011). However, the molecular mechanism for these associations are not known, as none of these genetic variants have been shown to be associated with expression differences (Williams *et al.* 2011). Given that TCF4 dominant-negative or haploinsufficiency results in PTHS, a syndrome with much more profound neurodevelopmental deficits than those observed in schizophrenia, the mechanism of schizophrenia risk associated with *TCF4* is presumably due to less extreme alterations in TCF4 expression at some unknown time point in development. It is also unclear whether the physiological phenotype related to cortical excitability is a feature of the *TCF4* risk factor associated with schizophrenia, but studies of cortical physiology in patients with schizophrenia and in their healthy siblings have implicated altered cortical excitability (Callicott 2003).

PTHS syndrome is characterized by variable symptomatology presumably because of allelic heterogeneity represented in the deletions/mutations, producing both haploinsufficiency and/or dominant-negative effects (Sepp *et al.* 2012). We suggest this expression deficiency leads to intrinsic excitability defects in part due to altered expression (i.e. derepression) of KCNQ1 and SCN10a. The pathological expression of these peripheral ion channels in the CNS, may create a unique opportunity to target these channels with therapeutic agents

without producing unwanted off-target effects on normal neuronal physiology, and we speculate that targeting these ion channels may ameliorate cognitive deficits observed in PTHS and potentially schizophrenia.

Experimental Procedures

Animals and *in utero* electroporation

Pregnant Wistar rats were obtained from Charles River Laboratories, Inc. and maintained by SoBran on a 12-hour light cycle and fed *ad libitum. In utero* electroporation was performed as previously described (Maher and Loturco 2012; Chen *et al.* 2014). Electroporation was performed on embryonic day 16 (E16) and gestation age was confirmed during surgery. All plasmids were used at a final concentration of 1.5μg/μl and the mPFC was targeted for transfection. Pregnant dams were returned to the same housing conditions after recovery from surgery, and after litters were born, transfected rats were used for experiments at days P18–24.

The mouse model used for Pitt-Hopkins syndrome (Sweatt 2013), were heterozygous for a deletion of the DNA-binding domain of the Transcription Factor 4 (B6;129-TCF4tm1Zhu/J; stock number 013598, Jackson Laboratory, Bar Harbor, ME, RRID:IMSR JAX:013598) (Zhuang *et al.* 1996). Control mouse experiments were conducted with wild-type littermates. Mice were maintained by SoBran on a 12-hour light cycle and fed *ad libitum*.

Electrophysiology

For all experiments, artificial cerebrospinal fluid (ACSF) was oxygenated (95% 02 and 5% CO2) and contained (in mM): 125 NaCl, 25 NaHCO3, 1.25 NaH2PO4, 3 KCl, 25 dextrose, 1 MgCl2, and 2 CaCl2, pH 7.3. Patch pipettes were fabricated from borosilicate glass (N51A, King Precision Glass, Inc.) to a resistance of 2–5 MΩ. For current- and voltage-clamp measurements pipettes were filled with (in mM): 125 potassium gluconate, 10 HEPES, 4 Mg-ATP, 0.3 Na-GTP, 0.1 EGTA, 10 phosophocreatine, adjusted to pH 7.3 with KOH. For generation of I/O curves, all cells were recorded from their inherent resting membrane potential. For AHP current experiments, synaptic currents were blocked with DL-2-amino-5-phosphopentanoic acid (D,L-AP5, 100μM, Ascent Scientific), 2,3, dioxo-6-nitro-1,2,3,4, tetrahydrobenzo-quinoxaline-7-sulfonamide (NBQX, 10μM) and SR-95531 (Gabazine, 5μM, Ascent Scientific). Ca2+-activated currents were blocked with Tetraethylammonium chloride (TEA, 1mM, Abcam), apamin (100nM, Abcam), and carbachol (10 μM, Abcam). Current signals were recorded with either a Multiclamp 700A (Molecular Devices) or an Axopatch 200B amplifier (Molecular Devices) and were filtered at 2 kHz using a built in Bessel filter and digitized at 10 kHz. Voltage signals were filtered and 2 kHz and digitized at 10kHz. Data were acquired using Axograph on a Dell PC. Data acquisition was terminated when series resistance was >15 MΩ. For voltage-clamp recordings, pyramidal cells were held at −60 mV. No holding current was used for current-clamp recordings.

shRNA constructs

Hairpin sequences were designed to target the 3′ UTR of *Tcf4* (shTCF4_2; GTTTCAGCATTCCCAATTA; nucleotide position 65507957 to 65507975; accession number NC_005117.4) and the open reading frame of *Tcf4* (shTCF4; AGAAACTAGACGACGACAA; nucleotide position 65503088-65503106; accession number NC_005117.4). The control hairpin (shCon) was designed to target DsRed (AGTTCCAGTACGGCTCCAA)(Duan *et al.* 2007). Sense and anti-sense oligonucleotides were designed, annealed, and cloned into the BbsI and XbaI sites of the mU6pro vector, where expression of short hairpin RNA was under the control of mouse U6 promoter.

CRISPR-Cas9

sgRNA was designed for spCas9 PAM recognition elements in a common exon of *Tcf4* (guide G ATAACGCCCGTGAGCGCCTG; nucleotide position 64692509 to 64692528), and off-target effects were minimized by using the online CRISPR-Cas9 design tool (http://CRISPR-Cas9.mit.edu/) with none predicted within any genes. A “G” was added to the sgRNA sequence for compatibility with U6 promoter. The annealed oligonucleotide was cloned into the BbsI site of the PX458 vector (Ran *et al.* 2013) (Addgene 48138) and sequenced for confirmation. The mis-match sensitive SURVEYOR nuclease assay was performed on genomic DNA extracted from neuroblastoma cells following manufacturer protocol (Transgenesis) 48hr post-transfection to confirm functional CRISPR-Cas9-mediated editing. pCAG-GFP plasmid was also used to verify transfection efficiency. To determine CRISPR-Cas9 generated mutations, purified DNA from transfected rat neuroblastoma cells was subjected to PCR amplification and TA cloning. Primers were designed using Primer3 software (http:/bioinfo.ut.ee/primer3-0.4.0/). Individual plasmid clones were purified and sequenced. In all experiments, a PX458 vector with no sgRNA guide (crEmpty) was used as a control.

iTRAP

TRAP was performed as previously described (Heiman *et al.* 2014) with the following additions described below. C2-EGFP-L10a was cloned into the XmaI and NotI sites of the pCAG-GFP plasmid (Addgene 11150) where expression for was under the control of the CAG promoter. Replicate tissue samples were prepared from three litters of 7–9 Wistar rats that had been transfected by *in utero* electroporation in mPFC with L10a-GFP plasmid and either shTCF4 or shCon. P22 rats were deeply anesthetized with isofluorane before transcardial perfusion with ice-cold buffer containing (in mM): 83 NaCl, 2.5 KCl, 1 NaH2PO4, 26.2 NaHCO3, 22 glucose, 72 sucrose, 0.5 CaCl2, and 3.3 MgCl2 (oxygenated with 95% O2 and 5% CO2). Rats were decapitated, and their brains removed and placed into dissection buffer containing cycloheximide. The transfected prefrontal cortex of each brain was dissected and all brains from a replicate litter were pooled into a Teflon-glass homogenizer and homogenized at 900rpm. Samples were cleared of nuclei and debris by centrifugation and incubated with detergents NP-40 (30mM) and DHPC (1%) for 5 minutes before a final 20,000g centrifugation for 15 minutes. Supernatant from each sample was then incubated for 1 hour at 4°C with protein-G coated magnetic beads (Invitrogen) conjugated to monoclonal anti-GFP antibodies (19C8 and 19F7, Rockefeller Univ.). Following

conjugation, supernatant was taken from the unbound fraction as an unbound total RNA control sample. Trizol reagent RNA extraction from samples was done following manufacturer protocol (Ambion). Samples were also purified by DNase treatment before concentration with RNeasy min-elute columns (Qiagen). RNA quantity was measured with an Invitrogen Qubit, and RNA quality was confirmed with an Agilent BioAnalyzer (RIN>8).

Supplementary Material

Refer to Web version on PubMed Central for supplementary material.

Acknowledgments

We are grateful for the vision and generosity of the Lieber and Maltz families, who made this work possible. We thank the families who donated to this research. Human brain material was acquired from the Offices of the Chief Medical Examiner of the District of Columbia, and of the Commonwealth of Virginia, Northern District, the National Institute of Child and Health Development Brain and Tissue Bank, and processed and stored at the NIH Clinical Center in Bethesda, Maryland. We thank M. Sepp and T. Timmusk for TCF4B expression construct; N Heintz for L10a-EGFP construct; T-P Su for B104 cells; J LoTurco for mu6 pro construct. This work was supported by the Lieber Institute, NIH (K01MH086050 and R56MH104593), NARSAD Young Investigator Award, and Pitt-Hopkins Research Foundation Award to B.J.M.

References

Abel HJ. Relationships Between Intracellular Calcium and Afterhyperpolarizations in Neocortical Pyramidal Neurons. Journal of Neurophysiology. 2003; 91:324–335. [PubMed: 12917389]

Alvarez VA, Ridenour DA, Sabatini BL. Retraction of synapses and dendritic spines induced by off-target effects of RNA interference. Journal of Neuroscience. 2006; 26:7820–7825. [PubMed: 16870727]

Amiel J, Rio M, de Pontual L, Redon R, Malan V, Boddaert N, Plouin P, et al. Mutations in TCF4, encoding a class I basic helix-loop-helix transcription factor, are responsible for Pitt-Hopkins syndrome, a severe epileptic encephalopathy associated with autonomic dysfunction. American journal of human genetics. 2007; 80:988–993. [PubMed: 17436254]

Baek ST, Kerjan G, Bielas SL, Lee JE, Fenstermaker AG, Novarino G, Gleeson JG. Off-target effect of doublecortin family shRNA on neuronal migration associated with endogenous microRNA dysregulation. Neuron. 2014; 82:1255–1262. [PubMed: 24945770]

Baker MD, Wood JN. Involvement of Na+ channels in pain pathways. Trends in pharmacological sciences. 2001; 22:27–31. [PubMed: 11165669]

Bean BP. The action potential in mammalian central neurons. Nature reviews Neuroscience. 2007; 8:451–465. [PubMed: 17514198]

Blair NT, Bean BP. Role of tetrodotoxin-resistant Na+ current slow inactivation in adaptation of action potential firing in small-diameter dorsal root ganglion neurons. Journal of Neuroscience. 2003; 23:10338–10350. [PubMed: 14614093]

Brockschmidt A, Filippi A, Charbel Issa P, Nelles M, Urbach H, Eter N, Driever W, et al. Neurologic and ocular phenotype in Pitt–Hopkins syndrome and a zebrafish model. Human Genetics. 2011; 130:645–655. [PubMed: 21544580]

Callicott JH. An expanded role for functional neuroimaging in schizophrenia. Current opinion in neurobiology. 2003; 13:256–260. [PubMed: 12744982]

Chen F, Maher BJ, Loturco JJ. PiggyBac Transposon-Mediated Cellular Transgenesis in Mammalian Forebrain by In Utero Electroporation. Cold Spring Harbor Protocols. 2014; 2014 pdb.prot073650–pdb.prot073650.

Consortium TEP. An integrated encyclopedia of DNA elements in the human genome. Nature. 2012; 489:57–74. [PubMed: 22955616]

Corneliussen B, Thornell A, Hallberg B, Grundström T. Helix-loop-helix transcriptional activators bind to a sequence in glucocorticoid response elements of retrovirus enhancers. Journal of virology. 1991; 65:6084–6093. [PubMed: 1681116]

de Pontual LC, Mathieu Y, Golzio C, Rio MN, Malan VR, Boddaert N, Soufflet C, et al. Mutational, functional, and expression studies of the TCF4gene in Pitt-Hopkins syndrome. Human Mutation. 2009; 30:669–676. [PubMed: 19235238]

Delmas P, Brown DA. Pathways modulating neural KCNQ/M (Kv7) potassium channels. Nature reviews Neuroscience. 2005; 6:850–862. [PubMed: 16261179]

Duan X, Chang JH, Ge S, Faulkner RL, Kim JY, Kitabatake Y, Liu XB, et al. Disrupted-In-Schizophrenia 1 regulates integration of newly generated neurons in the adult brain. Cell. 2007; 130:1146–1158. [PubMed: 17825401]

Flora A, Garcia JJ, Thaller C, Zoghbi HY. The E-protein Tcf4 interacts with Math1 to regulate differentiation of a specific subset of neuronal progenitors. Proceedings of the National Academy of Sciences of the United States of America. 2007; 104:15382–15387. [PubMed: 17878293]

Forrest M, Chapman RM, Doyle M, Tinsley CL, Waite A, Blake DJ. Functional analysis of TCF4 missense mutations that cause Pitt-Hopkins Syndrome. Human Mutation. 2012 n/a–n/a.

Goldberg TE, Weinberger DR. Probing prefrontal function in schizophrenia with neuropsychological paradigms. Schizophrenia Bulletin. 1988; 14:179–183. [PubMed: 3059467]

Goldman-Rakic PS. Cellular basis of working memory. Neuron. 1995; 14:477–485. [PubMed: 7695894]

Goldman-Rakic PS. Working memory dysfunction in schizophrenia. The Journal of neuropsychiatry and clinical neurosciences. 1994; 6:348–357. [PubMed: 7841806]

Grubišić V, Kennedy AJ, Sweatt JD, Parpura V. Pitt-Hopkins Mouse Model has Altered Particular Gastrointestinal Transits In Vivo. Autism research : official journal of the International Society for Autism Research. 2015

Gu N, Vervaeke K, Hu H, Storm JF. Kv7/KCNQ/M and HCN/h, but not KCa2/SK channels, contribute to the somatic medium after-hyperpolarization and excitability control in CA1 hippocampal pyramidal cells. The Journal of Physiology. 2005; 566:689–715. [PubMed: 15890705]

Guillemot F. Cell fate specification in the mammalian telencephalon. Progress in neurobiology. 2007; 83:37–52. [PubMed: 17517461]

Hawrylycz MJ, Lein ES, Guillozet-Bongaarts AL, Shen EH, Ng L, Miller JA, van de Lagemaat LN, et al. An anatomically comprehensive atlas of the adult human brain transcriptome. Nature. 2012; 489:391–399. [PubMed: 22996553]

Heiman M, Kulicke R, Fenster RJ, Greengard P, Heintz N. Cell type-specific mRNA purification by translating ribosome affinity purification (TRAP). Nature protocols. 2014; 9:1282–1291. [PubMed: 24810037]

Heiman M, Schaefer A, Gong S, Peterson JD, Day M, Ramsey KE, Suárez-Fariñas M, et al. A Translational Profiling Approach for the Molecular Characterization of CNS Cell Types. Cell. 2008; 135:738–748. [PubMed: 19013281]

Henthorn P, Kiledjian M, Kadesch T. Two distinct transcription factors that bind the immunoglobulin enhancer microE5/kappa 2 motif. Science (New York, NY). 1990; 247:467–470.

Hille B. Ion Channels of Excitable Membranes. 2001

Huang J, Yang Y, Zhao P, Gerrits MM, Hoeijmakers JGJ, Bekelaar K, Merkies ISJ, et al. Small-Fiber Neuropathy Nav1.8 Mutation Shifts Activation to Hyperpolarized Potentials and Increases Excitability of Dorsal Root Ganglion Neurons. The Journal of neuroscience : the official journal of the Society for Neuroscience. 2013; 33:14087–14097. [PubMed: 23986244]

Jentsch TJ. Neuronal KCNQ potassium channels:physislogy and role in disease. Nature reviews Neuroscience. 2000; 1:21–30. [PubMed: 11252765]

Ji H, Jiang H, Ma W, Johnson DS, Myers RM, Wong WH. An integrated software system for analyzing ChIP-chip and ChIP-seq data. Nature Biotechnology. 2008; 26:1293–1300.

Langevin LM, Mattar P, Scardigli R, Roussigné M, Logan C, Blader P, Schuurmans C. Validating in utero electroporation for the rapid analysis of gene regulatory elements in the murine telencephalon. Developmental dynamics : an official publication of the American Association of Anatomists. 2007; 236:1273–1286. [PubMed: 17377980]

Lein ES, Hawrylycz MJ, Ao N, Ayres M, Bensinger A, Bernard A, Boe AF, et al. Genome-wide atlas of gene expression in the adult mouse brain. Nature. 2007; 445:168–176. [PubMed: 17151600]

Lorenzon NM, Foehring RC. Alterations in intracellular calcium chelation reproduce developmental differences in repetitive firing and afterhyperpolarizations in rat neocortical neurons. Developmental brain research. 1995; 84:192–203. [PubMed: 7743638]

Maher, BJ.; Loturco, JJ. In Utero Electroporation for Cellular Transgenesis in the Developing Mammalian Forebrain. In: Morozov, A., editor. Neuromethods. Totowa, NJ: Humana Press; 2012. p. 113-128.

Massari ME, Murre C. Helix-Loop-Helix Proteins: Regulators of Transcription in Eucaryotic Organisms. Molecular and cellular biology. 2000; 20:429–440. [PubMed: 10611221]

McCleskey EW, Gold MS. ION CHANNELS OF NOCICEPTION. 2003; 61:835–856. dx.doi.org.

Powell LM, Jarman AP. Context dependence of proneural bHLH proteins. Current opinion in genetics & development. 2008; 18:411–417. [PubMed: 18722526]

Quednow BB, Ettinger U, Mossner R, Rujescu D, Giegling I, Collier DA, Schmechtig A, et al. The Schizophrenia Risk Allele C of the TCF4 rs9960767 Polymorphism Disrupts Sensorimotor Gating in Schizophrenia Spectrum and Healthy Volunteers. Journal of Neuroscience. 2011; 31:6684–6691. [PubMed: 21543597]

Ran FA, Hsu PD, Lin CY, Gootenberg JS, Konermann S, Trevino AE, Scott DA, et al. Double Nicking by RNA-Guided CRISPR Cas9 for Enhanced Genome Editing Specificity. Cell. 2013; 154:1380–1389. [PubMed: 23992846]

Sah P, Louise Faber ES. Channels underlying neuronal calcium-activated potassium currents. Progress in neurobiology. 2002; 66:345–353. [PubMed: 12015199]

Schizophrenia Psychiatric Genome-Wide Association Study (GWAS) Consortium. Genome-wide association study identifies five new schizophrenia loci. Nature Genetics. 2011; 43:969–976. [PubMed: 21926974]

Schizophrenia Working Group of the Psychiatric Genomics Consortium. Biological insights from 108 schizophrenia-associated genetic loci. Nature. 2014; 511:421–427. [PubMed: 25056061]

Sepp, M.; Kannike, K.; Eesmaa, A.; Urb, M.; Timmusk, T. Functional Diversity of Human Basic Helix-Loop-Helix Transcription Factor TCF4 Isoforms Generated by Alternative 5′ Exon Usage and Splicing. In: Kashanchi, F., editor. PLoS ONE. Vol. 6. 2011. p. e22138

Sepp M, Pruunsild P, Timmusk T. Pitt-Hopkins syndrome-associated mutations in TCF4 lead to variable impairment of the transcription factor function ranging from hypomorphic to dominant-negative effects. Human Molecular Genetics. 2012

Soh H, Tzingounis AV. The specific slow afterhyperpolarization inhibitor UCL2077 is a subtype-selective blocker of the epilepsy associated KCNQ channels. Molecular pharmacology. 2010; 78:1088–1095. [PubMed: 20843955]

Soileau B, Hasi M, Sebold C, Hill A, O'Donnell L, Hale DE, Cody JD. Adults with Chromosome 18 Abnormalities. Journal of genetic counseling. 2014; 24:1–12. [PubMed: 25432783]

Sweatt JD. Pitt-Hopkins Syndrome: intellectual disability due to loss of TCF4-regulated gene transcription. Experimental & molecular medicine. 2013; 45:e21. [PubMed: 23640545]

Towart R, Linders JTM, Hermans AN, Rohrbacher J, van der Linde HJ, Ercken M, Cik M, et al. Blockade of the IKs potassium channel: An overlooked cardiovascular liability in drug safety screening? Journal of Pharmacological and Toxicological Methods. 2009; 60:1–10. [PubMed: 19439185]

Tyler WA, Medalla M, Guillamon-Vivancos T, Luebke JI, Haydar TF. Neural Precursor Lineages Specify Distinct Neocortical Pyramidal Neuron Types. The Journal of neuroscience : the official journal of the Society for Neuroscience. 2015; 35:6142–6152. [PubMed: 25878286]

Tzingounis AV, Nicoll RA. Contribution of KCNQ2 and KCNQ3 to the medium and slow afterhyperpolarization currents. Proceedings of the National Academy of Sciences. 2008; 105:19974–19979.

Tzingounis AV, Kobayashi M, Takamatsu K, Nicoll RA. Hippocalcin Gates the Calcium Activation of the Slow Afterhyperpolarization in Hippocampal Pyramidal Cells. Neuron. 2007; 53:487–493. [PubMed: 17296551]

Vijayaragavan K, O'Leary ME, Chahine M. Gating properties of Na(v)1.7 and Na(v)1.8 peripheral nerve sodium channels. Journal of Neuroscience. 2001; 21:7909–7918. [PubMed: 11588164]

Vogalis F, Storm JF, Lancaster B. SK channels and the varieties of slow after-hyperpolarizations in neurons. European Journal of Neuroscience. 2003; 18:3155–3166. [PubMed: 14686890]

Whalen S, Heron D, Gaillon T, Moldovan O, Rossi M, Devillard F, Giuliano F, et al. Novel comprehensive diagnostic strategy in Pitt-Hopkins syndrome: clinical score and further delineation of the TCF4 mutational spectrum. Human Mutation. 2012; 33:64–72. [PubMed: 22045651]

Williams HJ, Moskvina V, Smith RL, Dwyer S, Russo G, Owen MJ, O'Donovan MC. Association between TCF4 and schizophrenia does not exert its effect by common nonsynonymous variation or by influencing cis-acting regulation of mRNA expression in adult human brain. American Journal of Medical Genetics Part B: Neuropsychiatric Genetics. 2011; 156:781–784.

Zhu X, Gu H, Liu Z, Xu Z, Chen X, Sun X, Zhai J, et al. Associations between TCF4 Gene Polymorphism and Cognitive Functions in Schizophrenia Patients and Healthy Controls. Neuropsychopharmacology : official publication of the American College of Neuropsychopharmacology. 2012; 38:683–689. [PubMed: 23249814]

Zhuang Y, Cheng P, Weintraub H. B-lymphocyte development is regulated by the combined dosage of three basic helix-loop-helix genes, E2A, E2-2, and HEB. Molecular and cellular biology. 1996; 16:2898–2905. [PubMed: 8649400]

Zweier C, Sticht H, Bijlsma EK, Clayton-Smith J, Boonen SE, Fryer A, Greally MT, et al. Further delineation of Pitt-Hopkins syndrome: phenotypic and genotypic description of 16 novel patients. Journal of medical genetics. 2008; 45:738–744. [PubMed: 18728071]

Highlights

- TCF4 loss of function alters the intrinsic excitability of prefrontal neurons.
- TCF4-dependent excitability deficits are rescued by SCN10a and KCNQ1 antagonists.
- TCF4 represses the expression of SCN10a and KCNQ1 ion channels in central neurons.
- SCN10a is a potential therapeutic target for Pitt Hopkins syndrome.

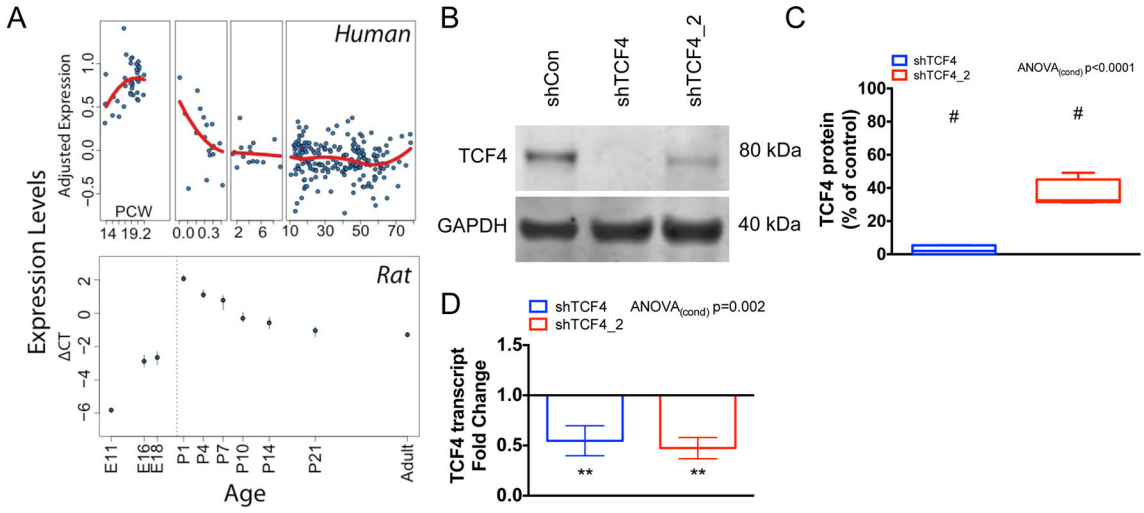

Figure 1.

Developmental expression pattern and shRNA knockdown of TCF4. (**A**) Comparison of the lifespan expression patterns of TCF4 between humans and rats. Human DLPFC expression data for TCF4 on 269 individuals across the lifespan was obtained from: http://braincloud.jhmi.edu/plots/ Red: smoothing spline (upper panel). qRT-PCR analysis of *Tcf4* transcripts obtained from rat cortical samples (lower panel). (**B–D**) *In vitro* validation of TCF4 shRNAs to effectively knockdown TCF4 expression. (**B,C**) Rat neuroblastoma cells were transfected with shRNA constructs and an equal amount of cell lysate sample from each condition was subjected to Western blot analysis for endogenous TCF4 protein (shTCF4 = 1.9±2.0% of control, N=4, Bonferroni p<0.0001; shTCF4_2 = 36.4±4.3% of control, N=4, Bonferroni p<0.0001). (**D**) Rat neuroblastoma cells were transfected with shRNA constructs and subjected to qRT-PCR for *Tcf4* transcript (shTCF4 = 0.55±0.15 fold change from control, N=4, Bonferroni p=0.0065; shTCF4_2 0.47±0.11 fold change from control, N=4, Bonferroni p=0.0017). Values are presented as Tukey boxplots and statistical significance via Bonferroni *post hoc* analysis (** p<0.01, # p<0.0001).

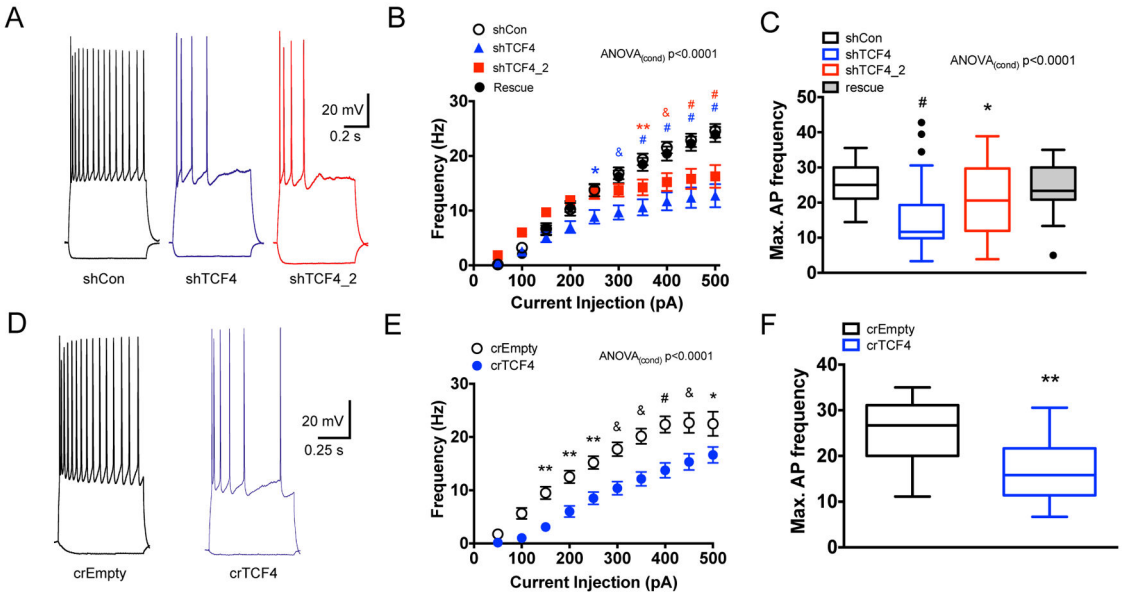

Figure 2.

TCF4 regulates intrinsic excitability of L2/3 pyramidal cells of the mPFC. (**A,B**) *In utero* shRNA knockdown of TCF4 prevents neurons from displaying repetitive spiking. Shown in (**A**) are sample current-clamp traces recorded from EGFP+ neurons expressing shCon, shTCF4, or shTCF4_2 in response to 600 ms current injections (+300 and -50pA). (**B**) Summary data of the frequency of APs generated in response to current injections. *Post hoc* analysis indicated that shTCF4 cells (N=30) between 250 and 500pA and shTCF4_2 cells N=41 between 350 and 500pA produced significantly fewer spikes than shCon cells (N=35). Co-expression of human TCF4B + shTCF4 (**B,C**) resulted in a complete rescue of AP output and *post hoc* analysis revealed no statistical difference between rescue cells (N=25) and shCon cells (N=35) at any current injection. (**C**) Group data depicting the maximum AP frequency obtained from each neuron from all conditions. *Post hoc* comparisons of the maximum AP frequency indicated that shTCF4 (15.79±1.8Hz, N=30; Bonferroni $p<0.0001$) and shTCF4_2 (20.77±1.5Hz, N=41; Bonferroni $p=0.032$) were significantly reduced compared to shCon (25.51±1.04Hz, N=35). (**D,E**) *In utero* knockout of TCF4 by CRISPR-Cas9-mediated mutation prevents neurons from displaying repetitive spiking. Shown in (**D**) are sample current-clamp traces recorded from EGFP+ neurons expressing crEmpty or crTCF4 in response to 600ms current injections (+300 and −50pA). (**E**) Summary data of the frequency of APs generated in response to current injections. crTCF4 produced a significant reduction in the frequency neuronal spiking compared to crEmpty cells. *Post hoc* analysis indicated that crTCF4 cells (N=20) between 150 and 500pA produced significantly fewer spikes than crEmpty cells (N=17). (**F**) Group data depicting the maximum AP frequency obtained from each neuron in each condition. The maximum spiking frequency analysis showed that crTCF4 cells (16.89±1.54Hz, N=20; unpaired t-test $p=0.0016$) were significantly reduced compared to crEmpty cells (24.90±1.78Hz, N=17). Values are presented as mean ± SEM (**B,E)** or Tukey boxplots (**C,F)** and statistical significance via Bonferroni *post hoc* analysis (**B,C,E**) or unpaired t-test (**F**) (* $p<0.05$, ** $p<0.01$, & $p<0.001$ # $p<0.0001$).

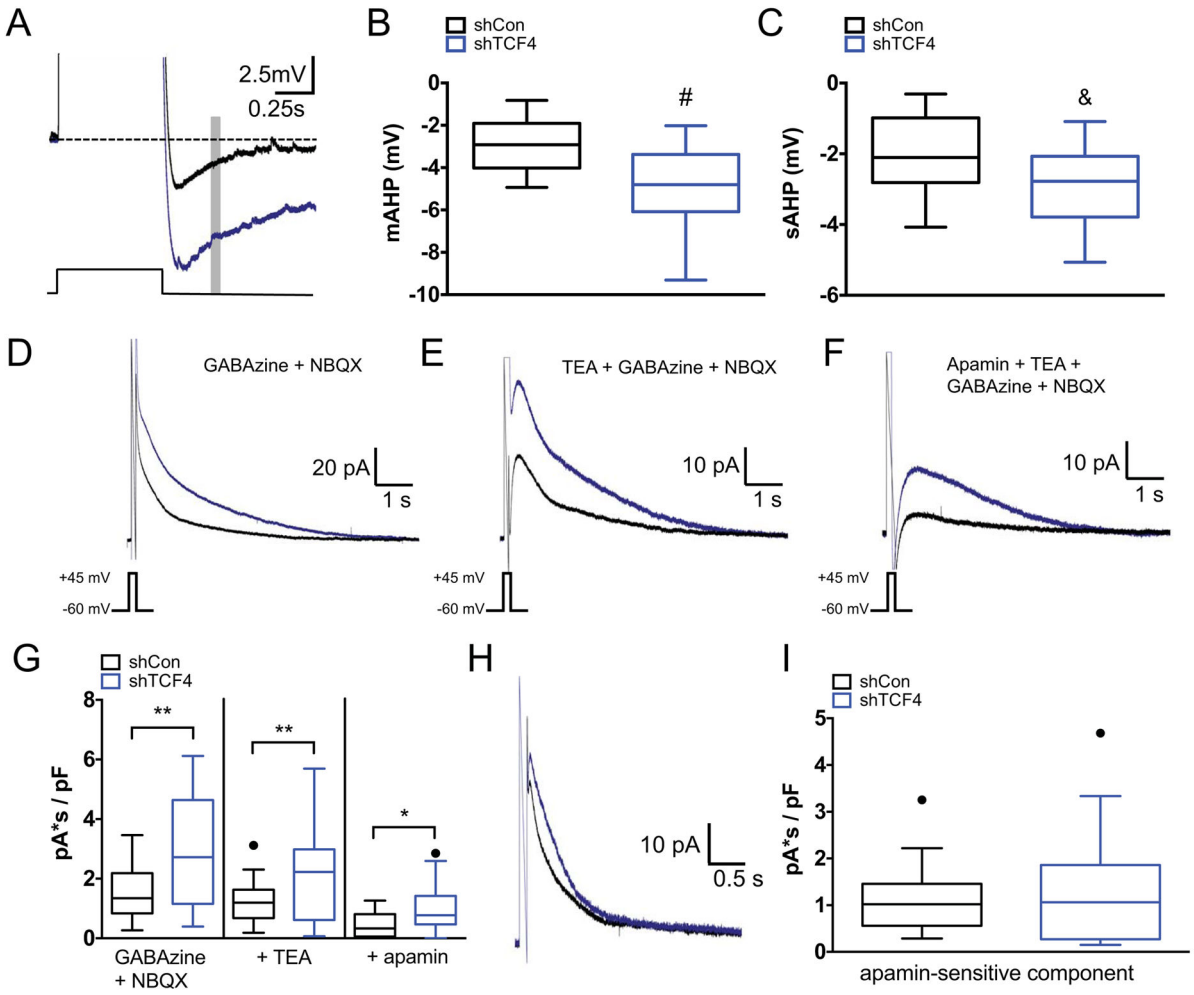

Figure 3.

TCF4 regulates the afterhyperpolarization potential. (**A–C**) Suppression of TCF4 results in an increase in the medium and slow AHP potential. Shown in (**A**) is a sample current-clamp traces highlighting the AHP that follows a train of APs produced by a 600ms current pulse. (**B**) Summary data comparing the peak amplitude of the mAHP from EGFP+ neurons expressing either shCon or shTCF4 constructs (shTCF4 = −4.76±0.35mV, N=26 vs. shCon = −2.98±0.24mV, N=26); unpaired t-test p<0.0001). The mAHP was measured at the peak of AHP following the current pulse. (**C**) Summary data comparing the amplitude of the sAHP obtained from EGFP+ neurons expressing either shCon or shTCF4 constructs (shTCF4 = −2.94±0.19mV, N=26 vs. shCon = −1.89±0.19mV, N=26; unpaired t-test p=0.0003). The sAHP was measured 280ms after the current pulse. (**D–H**) Whole-cell voltage-clamp recordings of AHP currents produced by applying 100ms voltage steps to +45 mV. Shown are average traces from all recordings from EGFP+ cells expressing shCon (black traces) or shTCF4 (blue traces). Shown if (**D**) is the baseline AHP current produced in the presence of the GABA and glutamate antagonists, gabazine and NBQX, respectively. Average traces showing progressive blockade of the fAHP current (**E**) by bath application of TEA, followed by blockade of the mAHP current with apamin (**F**). (**G**) Summary data showing the total

charge transfer obtained from all recorded neurons in each pharmacological condition. All data was normalized by the cells capacitance (pF). (**H**) Average subtracted traces before and after application of apamin (panel **E** minus panel **F**). (**I**) Summary data comparing only the apamin-sensitive component of the AHP currents between EGFP+ cells expressing either shCon or shTCF4. Values are presented as Tukey boxplots and statistical significance obtained via unpaired t-test (* $p<0.05$, ** $p<0.01$, & $p<0.001$ # $p<0.0001$).

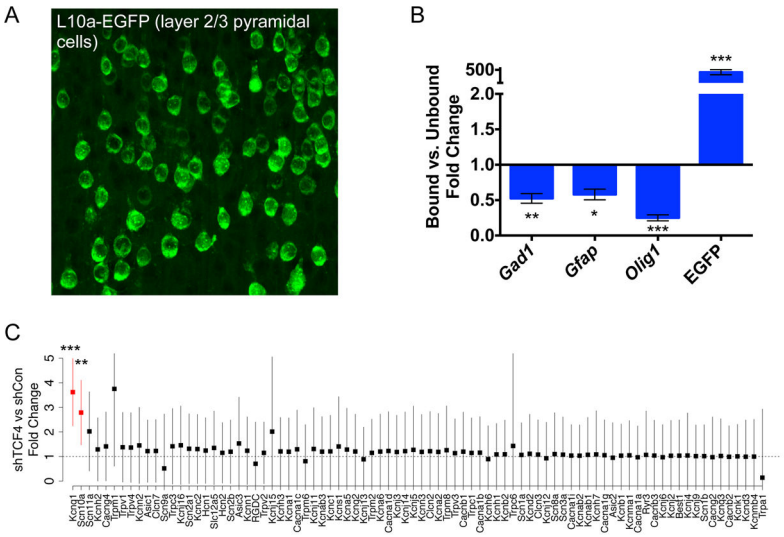

Figure 4.

iTRAP: Molecular profiling of the translatome identifies *KCNQ1* and *SCN10a*. (**A**) Sample image of mPFC L2/3 neurons IUE transfected with the ribosomal subunit L10a-EGFP. (**B**) iTRAP protocol enriches RNA from IUE transfected excitatory neurons. qRT-PCR comparison of the affinity purified RNA (bound) vs. the unbound fraction of RNA for cellular markers of interneurons (GAD1 fold-change 0.52±0.07, N=4; paired t-test p=0.007), astrocytes (GFAP fold-change 0.58±0.08, N=4; paired t-test p=0.01), oligodendrocytes (OLIG1 fold-change 0.25±0.04, N=4; paired t-test p=0.0003) and transfection marker (EGFP fold-change 408.9±95.9, N=4; paired t-test p=0.0006). (**C**) Comparison of the ion channel translatome between shTCF4 and shCon cells. Shown is the fold-change difference in expression between knockdown and control mPFC brain tissue ordered by p-values. Values are presented mean ± SEM statistical significance via Bonferroni *post hoc* analysis (* p<0.05, ** p<0.01, *** p<0.001).

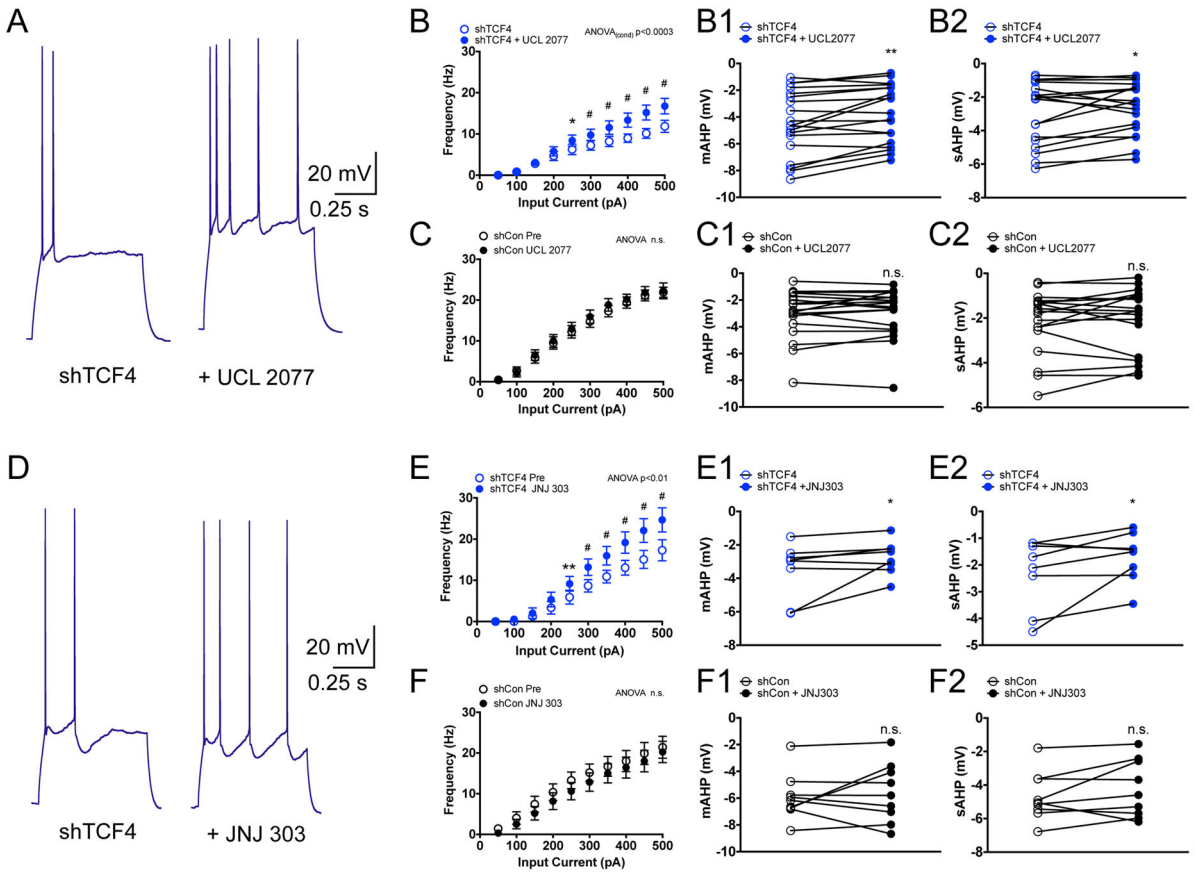

Figure 5.

Pharmacological block of KCNQ1 rescues phenotypes associated with suppression of TCF4. (**A**) Representative current-clamp traces from an shTCF4 cell showing the effect of UCL2077 (10μM) on the frequency of AP spiking. (**B**) Summary data of the effect of UCL2077 application on the frequency of APs in shTCF4 cells generated in response to current injections (N=17). *Post hoc* analysis indicates UCL2077 significantly increased firing frequency for current pulses between 250 and 500pA. (**B1**,**B2**) Before and after plots depicting the effect of UCL2077 application on the amplitudes of the mAHP (before −4.43±0.55mV vs. after −3.736±0.49mV, N=19, paired t-test p=0.003) and sAHP (before −2.88±0.42mV vs. after −2.53±0.38mV, N=19, paired t-test p<0.05) on shTCF4 cells. (**c**) Summary data of the effect of UCL2077 application on the frequency of APs in shCon cells generated in response to increasing current injections (N=8). (**C1**,**C2**) Before and after plots depicting the effect of UCL2077 application on the amplitudes of the mAHP (before −3.78±0.66mV vs. after −4.01±0.66mV, N=9, paired t-test p=0.20) and sAHP (before −2.60±0.42mV vs. after −2.69±0.48mV, N=9, paired t-test p=0.68) on shCon cells. (**D**) Representative current-clamp traces from an shTCF4 cell showing the effect of JNJ303 (1uM) on the frequency of AP spiking. (**E**) Summary data of the effect of JNJ303 application on the frequency of APs in shTCF4 cells generated in response to current injections (N=8). *Post hoc* analysis indicates JNJ303 significantly increased firing frequency for current pulses between 250 and 500pA. (**E1**,**E2**) Before and after plots depicting the effect of JNJ303 application on the amplitudes of the mAHP (before −3.52±0.58mV vs.

after −2.77±0.36mV, N=8, paired t-test p<0.044 and sAHP (before −2.31±0.46mV vs. after −1.71±0.33mV, N=8, paired t-test p=0.041) on shTCF4 cells. (**F**) Summary data of the effect of JNJ303 application on the frequency of APs in shCon cells generated in response to increasing current injections (N=8). (**F1**,**F2**) Before and after plots depicting the effect of JNJ303 application on the amplitudes of the mAHP (before −5.93±0.58mV vs. −5.61±0.74mV, N=9, paired t-test p=0.91) and sAHP (before −4.67±0.48mV vs. after −4.22±0.57, N=9, paired t-test p=0.20) on shCon cells.

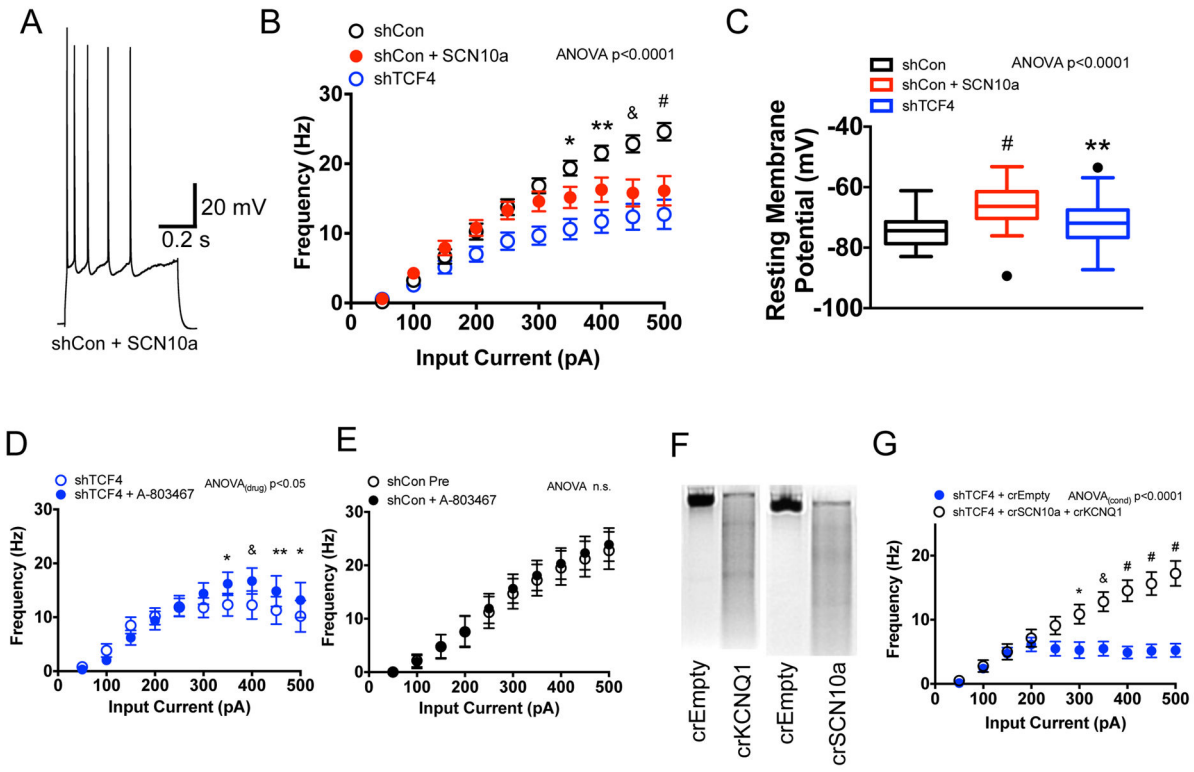

Figure 6.

Molecular and pharmacological validation of the role of SCN10a underlying intrinsic excitability phenotypes in shTCF4 cells. (**A**) Sample current-clamp trace showing the effect of co-expressing SCN10a in an shCon cell on AP spiking. (**B**) Summary data of the effect of co-expressing SCN10a + shCon on the frequency of APs generated in response to increasing current injections. *Post hoc* analysis indicates that SCN10a expression significantly decreases firing for current pulses between 350 and 500pA. (**C**) Summary plot showing the effect co-expression of SCN10a + shCon on the resting membrane potential (68.86±1.50mV, N=29; *post hoc* p=0.0005). (**D**) Summary data of the effect of A-803467 (200nM) application on the frequency of APs in shTCF4 cells generated in response to increasing current injections (N=11). *Post hoc* analysis indicates that A-803467 significantly increased firing for current pulses between 350 and 500pA. (**E**) Summary data of the effect of A-803467 application on the frequency of APs in shCon cells generated in response to increasing current injections (N=7). For statistical comparisons in panel **B** and **C**, shCon and shTCF4 data are the same datasets shown in Figure 2 and Figure S3. Values are presented as Tukey boxplots and statistical significance via Bonferroni *post hoc* analysis (* p<0.05, ** p<0.01, & p<0.001, # p<0.0001). (**F**) SURVEYOR assay showing CRISPR-Cas9 mediated mutation of *Kcnq1* and *Scn10a*. (**G**) Summary data of the effect of co-expressing shTCF4 + crSCN10a + crKCNQ1 on the frequency of APs generated in response to increasing current injections. *Post hoc* analysis indicates that CRISPR-Cas9 mediated mutation of *Scn10a* and *Kcnq1* significantly rescues AP firing for current pulses between 300pA and 500pA compared to co-expression of shTCF4 + crEmpty.

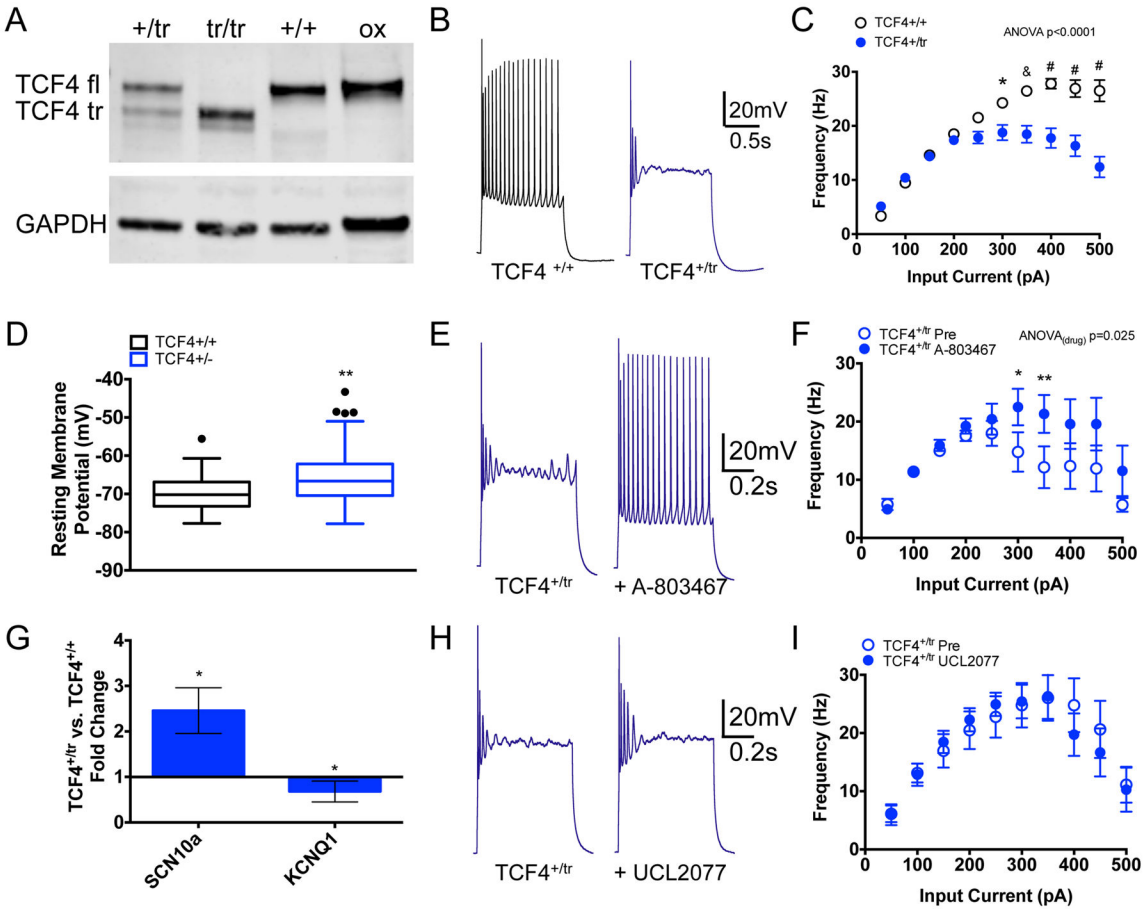

Figure 7.

Germline truncation of one allele of TCF4 phenocopies cell-autonomous knockdown of TCF4. Shown in (**A**) is a Western blot of TCF4 from E18 brain lysates. A single full-length TCF4 (TCF4fl) protein band is observed in lysates from wild-type (+/+) mouse brain and from expression of recombinant TCF4B (ox) in rat neuroblastoma cells. A truncated TCF4 (TCF4tr) protein is observed in lysates from heterozygous (+/tr) and knockout (tr/tr) mouse brain. Shown in (**B**) are sample whole-cell current-clamp traces recorded from mPFC layer 2/3 neurons from a $TCF4^{+/tr}$ and a wild-type littermate ($TCF4^{+/+}$) in response to 600 ms current injections (+450pA). (**C**) Summary data of the frequency of APs generated in response to current injections. *Post hoc* analysis indicated that $TCF^{+/tr}$ cells (N=46) between 300 and 500pA produced significantly fewer spikes than $TCF4^{+/+}$ cells (N=35). (**D**) Summary data showing the resting membrane potential is significantly depolarized in $TCF4^{+/tr}$ neurons versus $TCF4^{+/+}$ neurons. (**E**) Representative current-clamp traces from a $TCF4^{+/tr}$ cell showing the effect of A-803467 on the frequency of AP spiking. (**F**) Summary data of the effect of A-803467 application on the frequency of APs in $TCF4^{+/tr}$ cells generated in response to current injections (N=8). *Post hoc* analysis indicates A-803467 significantly increased firing frequency for current pulses between 250 and 350pA. (**G**) Summary qRT-PCR data showing increased expression of *Scn10a* and decreased expression of *Kcnq1* in the frontal cortex of $TCF4^{+/tr}$ mice compare to $TCF4^{+/+}$ mice. (**H**) Representative current-clamp traces from a $TCF4^{+/tr}$ cell showing UCL2077 has no effect on

the frequency of AP spiking. (**I**) Summary data of the effect of UCL2077 application on the frequency of APs in TCF4$^{+/tr}$ cells generated in response to current injections (N=8). Values are presented as mean ± SEM and statistical significance via Bonferroni *post hoc* analysis (* $p<0.05$, ** $p<0.01$, & $p<0.001$, # $p<0.0001$).